Supplementary Information

Comparative DNA Binding abilities and Phosphatase-like activities of Mono, Di and Trinuclear Ni(II) complexes: The Influence of Ligand Denticity, Metal-Metal Distance and Coordinating Solvent/ Anion on Kinetic Studies

Vimal K. Bhardwaj,[†] and Ajnesh Singh[‡]*

[†]Department of Chemistry, Indian Institute of Technology Ropar, Rupnagar, Punjab, 140001, India.

[‡]Department of Applied Science & Humanities, Jawaharlal Nehru Govt. Engineering College, Sundernagar, Mandi (H.P.)-175010, India.

Table of Contents

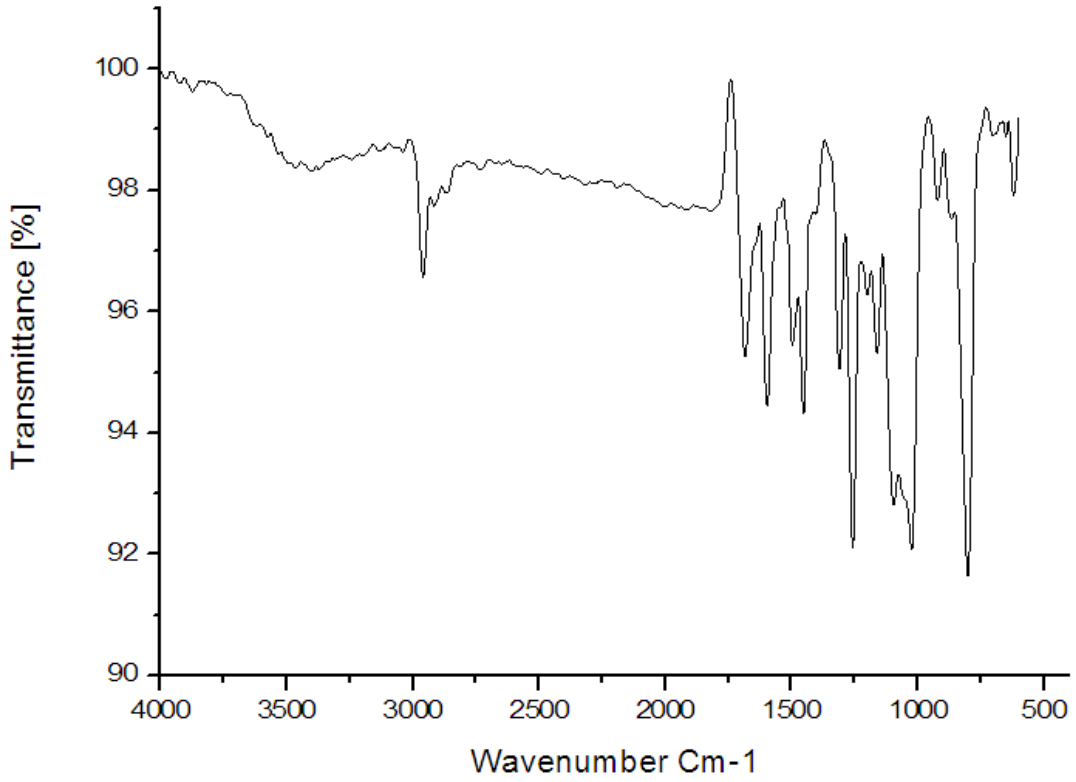

Figure S1. I.R. spectrum of complex **1**

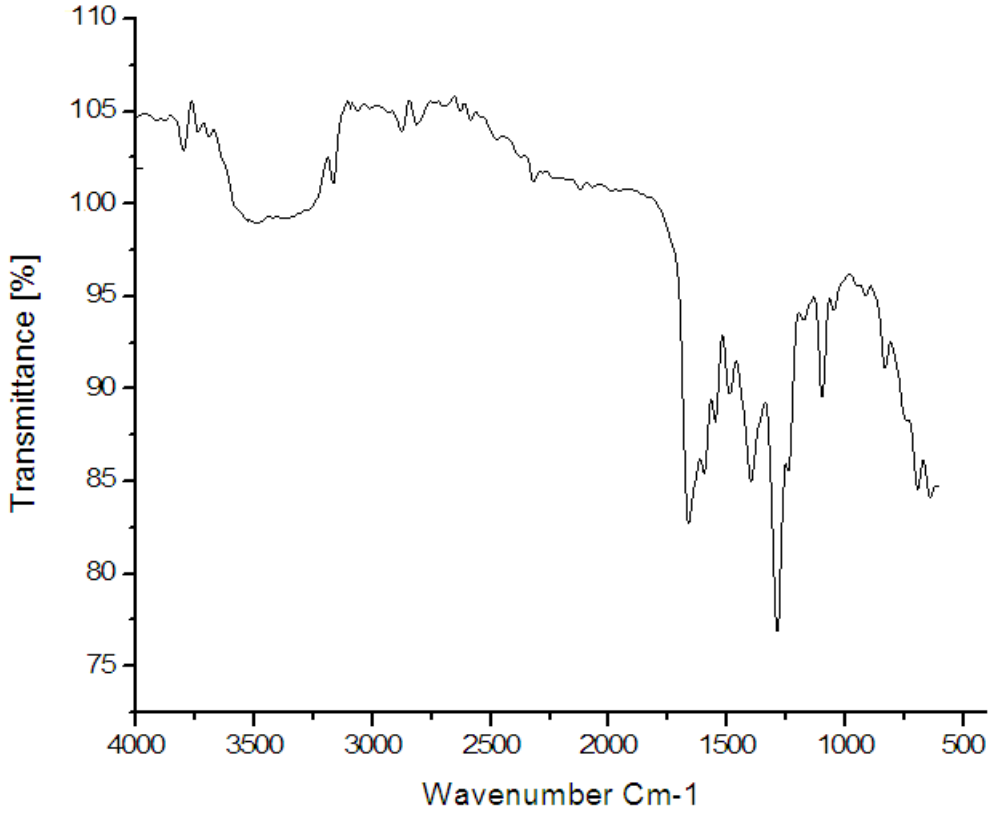

Figure S2. I.R. spectrum of complex **2**

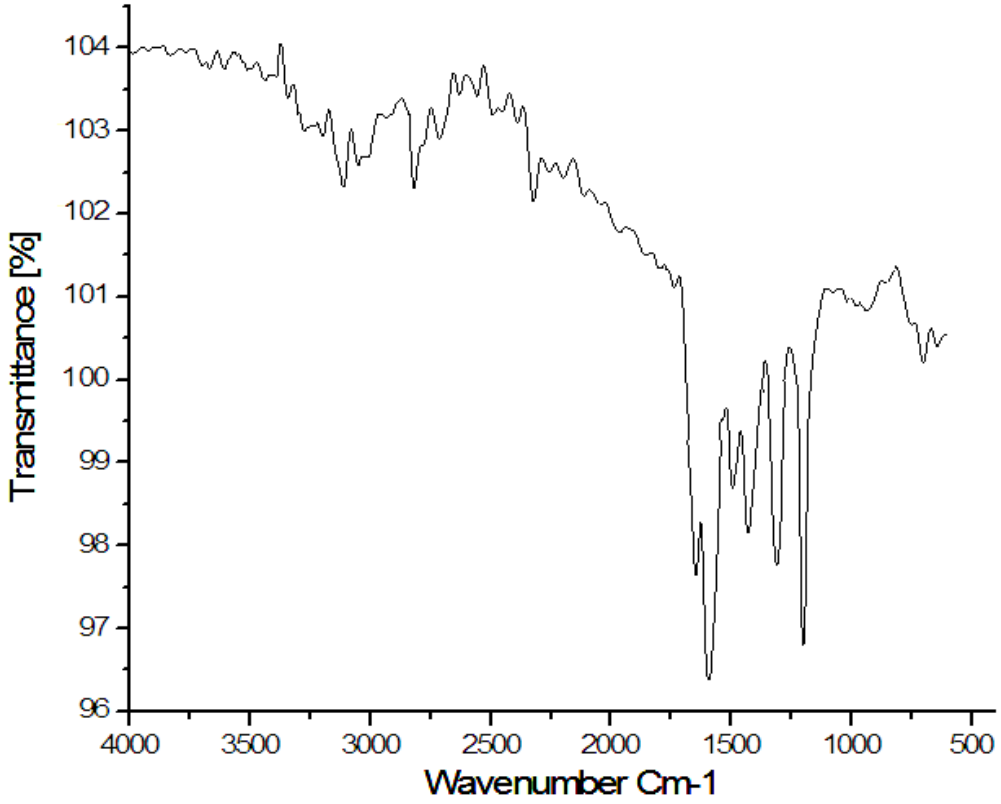

Figure S3. I.R. spectrum of complex **3**

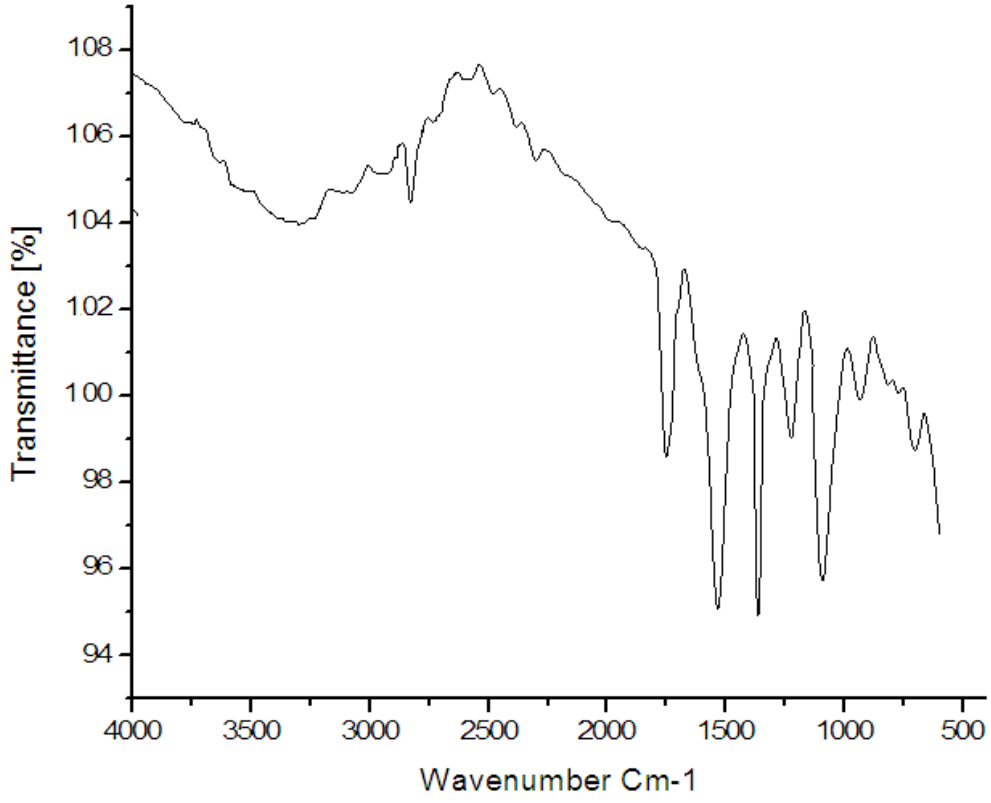

Figure S4. I.R. spectrum of complex **4**

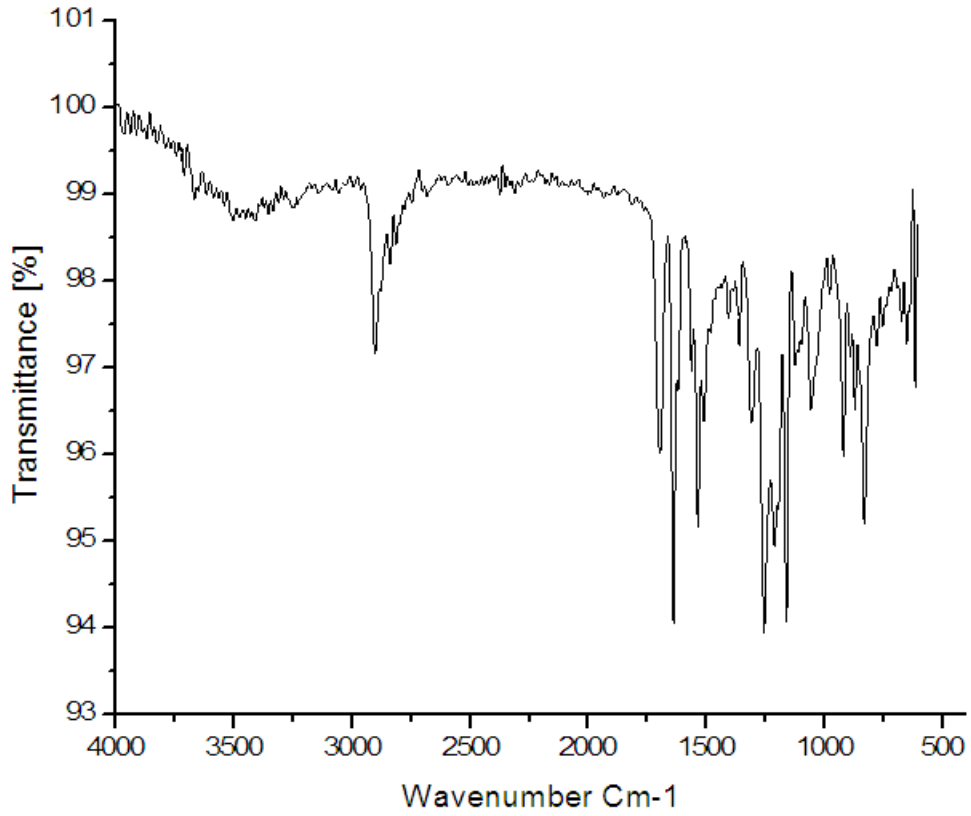

Figure S5. I.R. spectrum of complex **5**

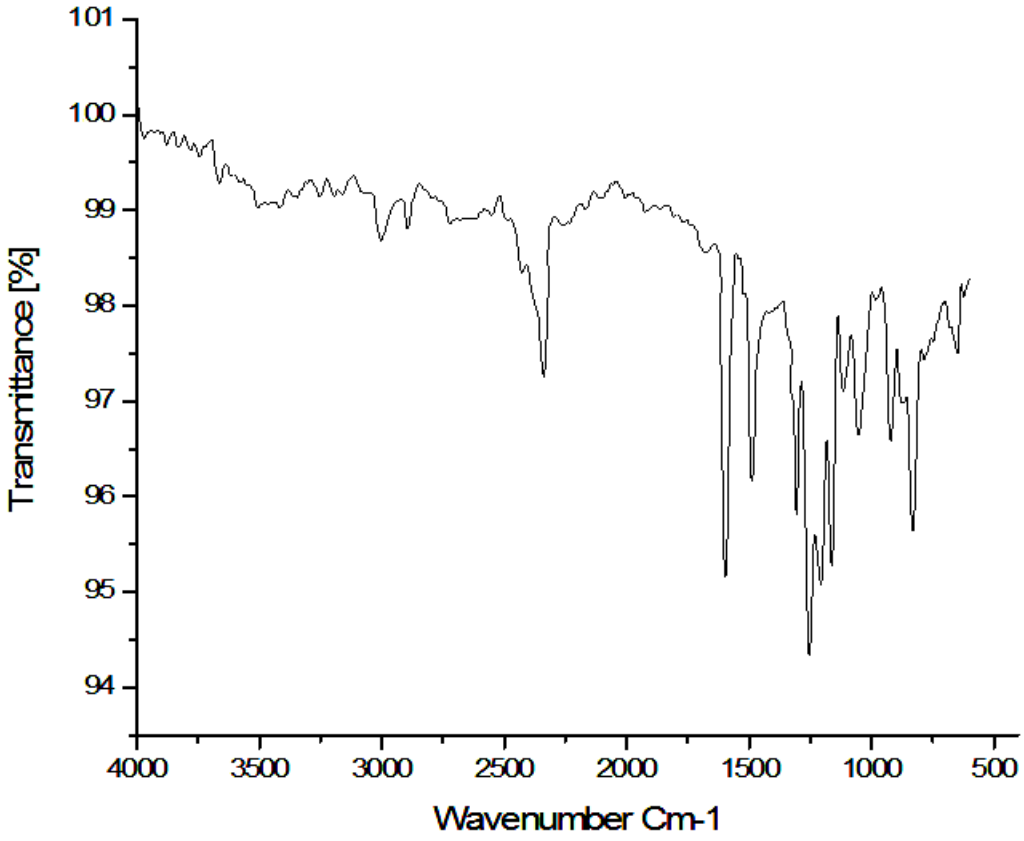

Figure S6. I.R. spectrum of complex **6**

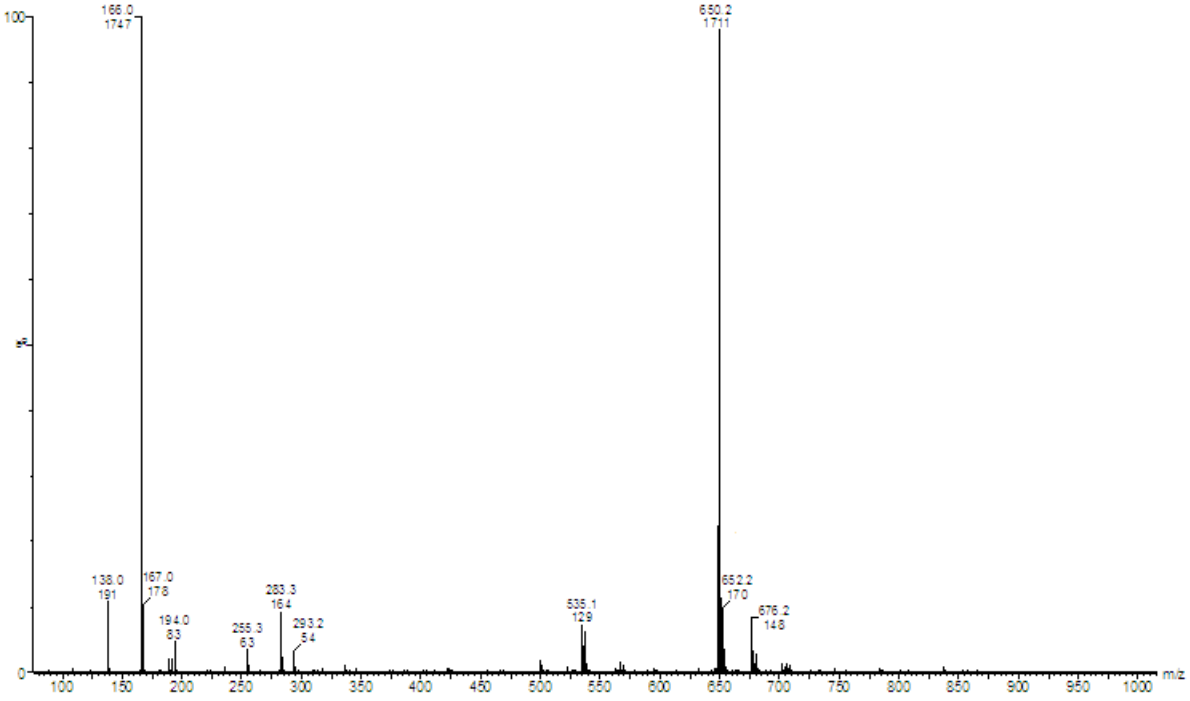

Figure S7. ESI-MS spectrum of complex **1**

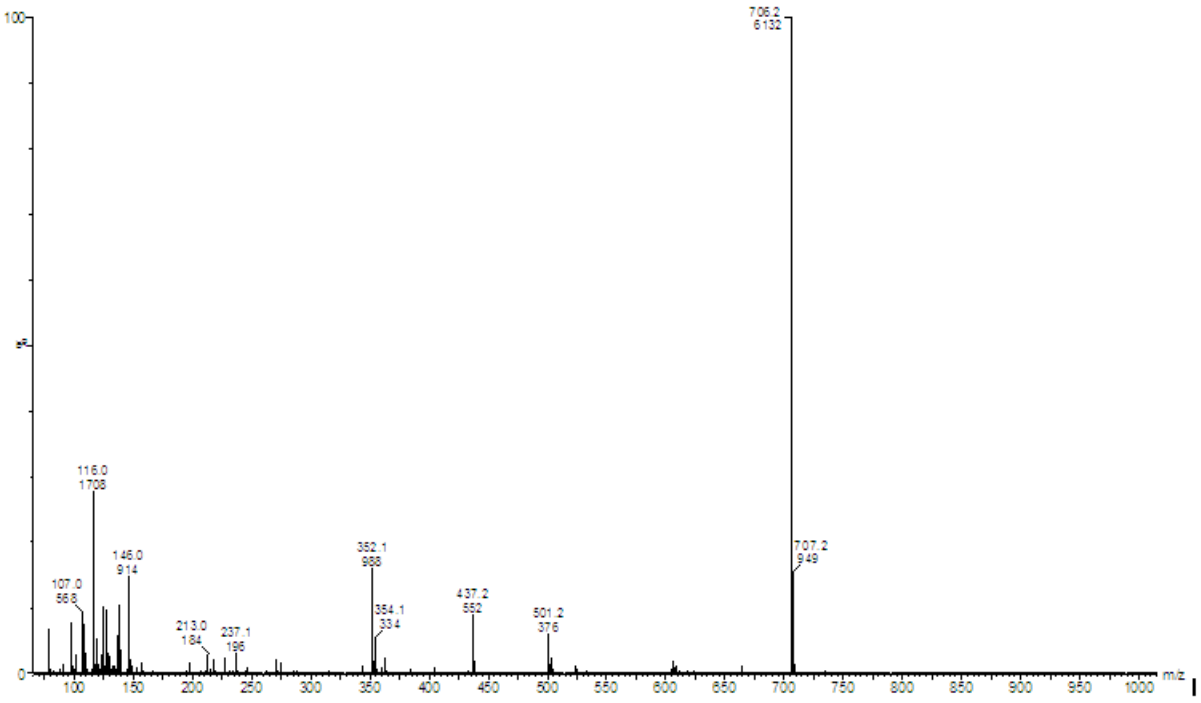

Figure S8. ESI-MS spectrum of complex **2**

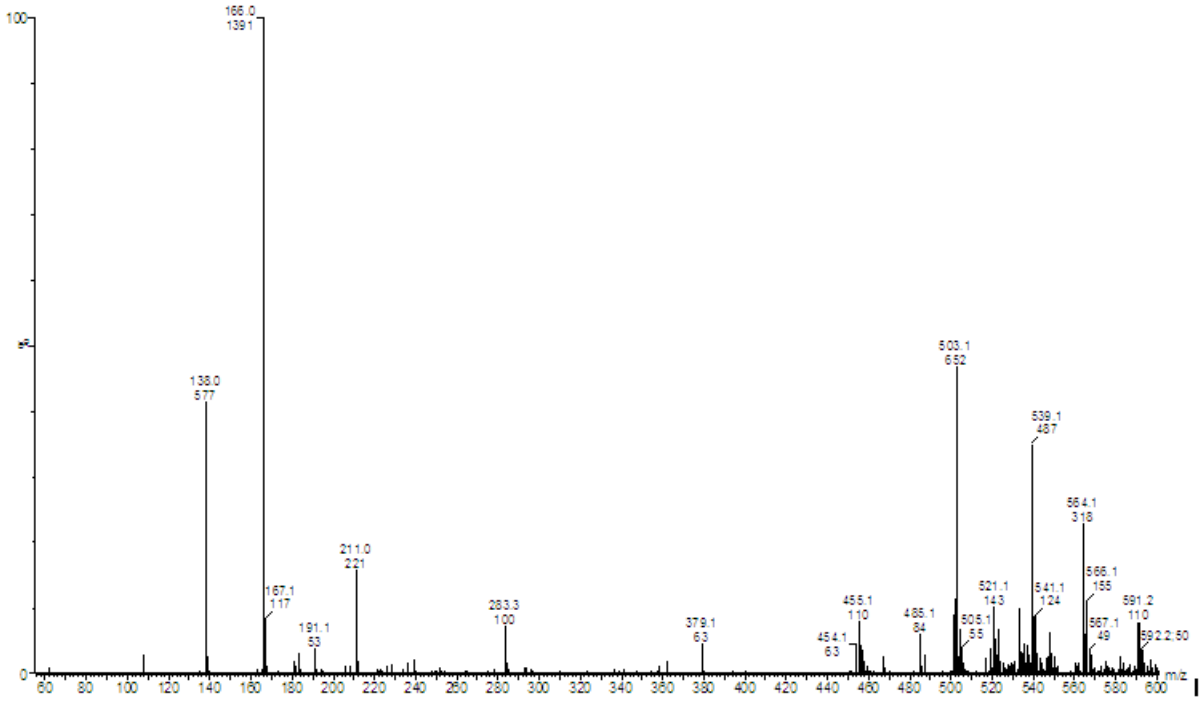

Figure S9. ESI-MS spectrum of complex **3**

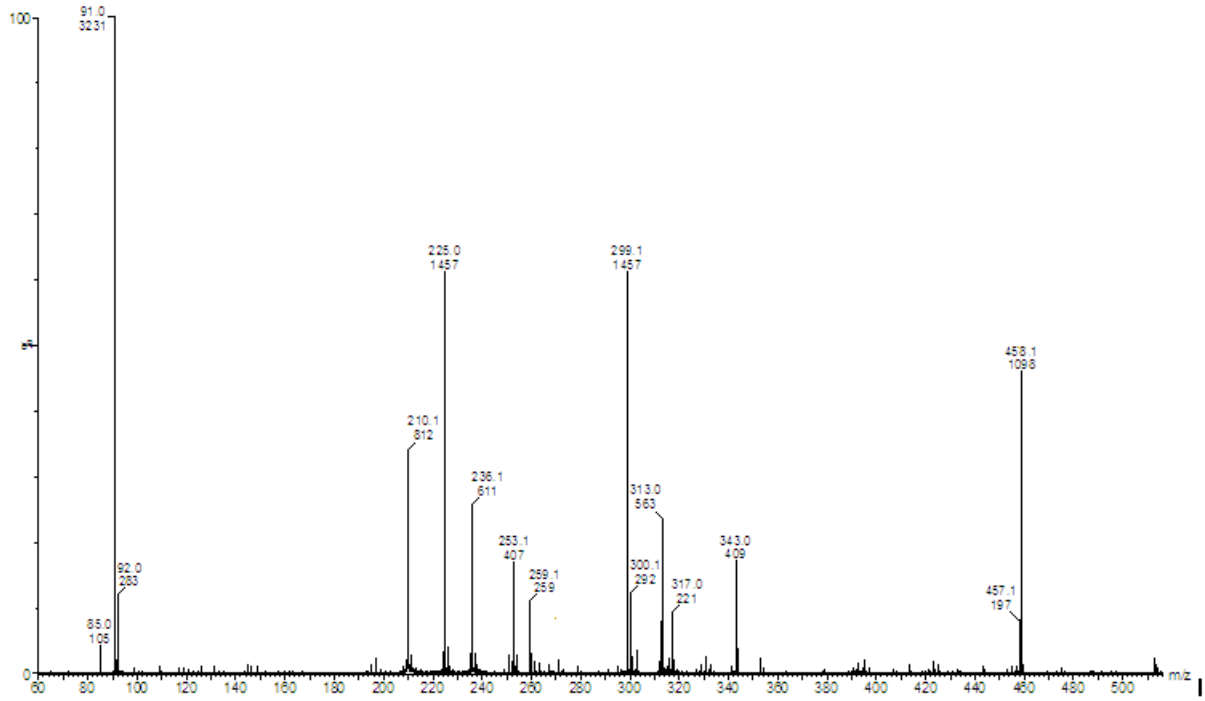

Figure S10. ESI-MS spectrum of complex **4**

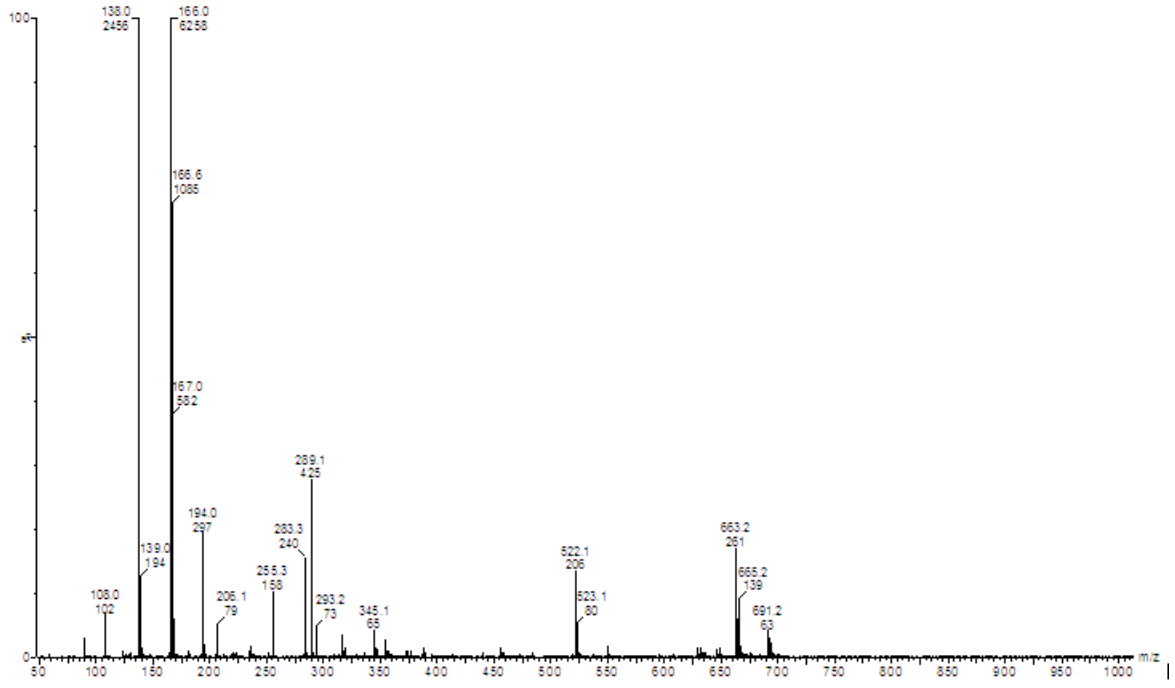

Figure S11. ESI-MS spectrum of complex **5**

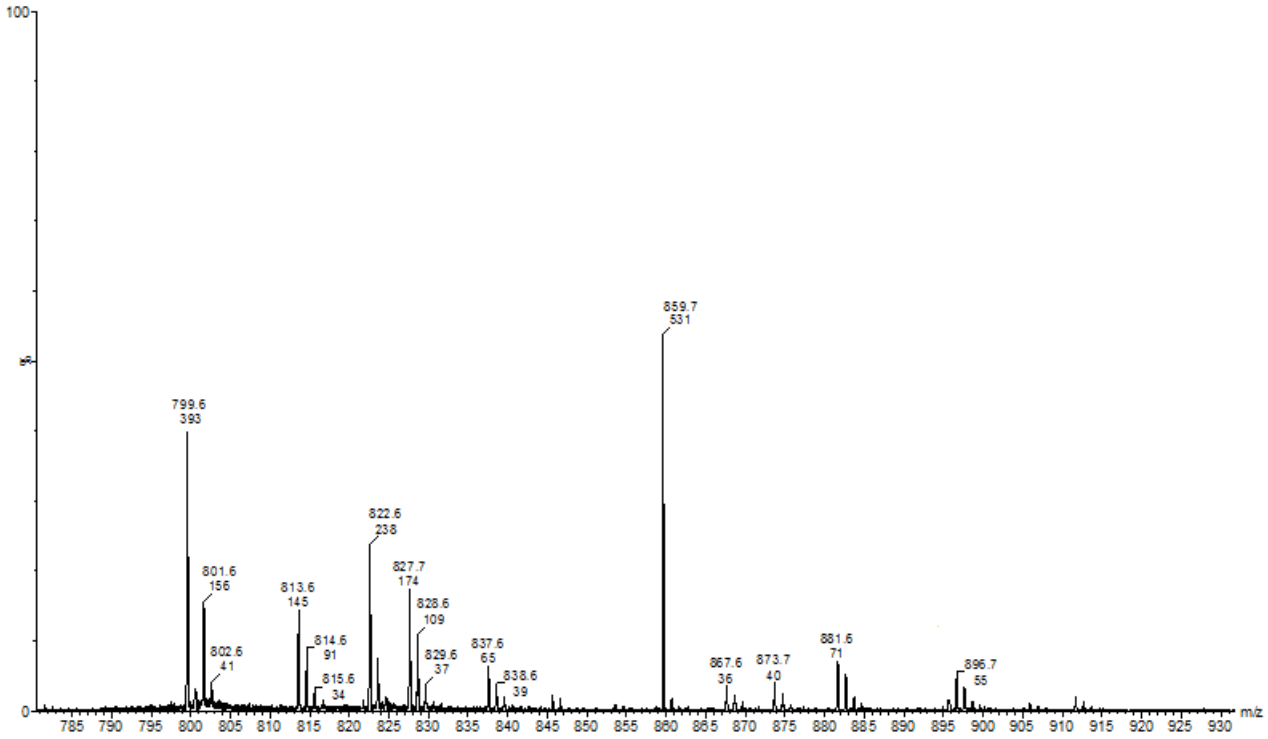

Figure S12. ESI-MS spectrum of complex **6**

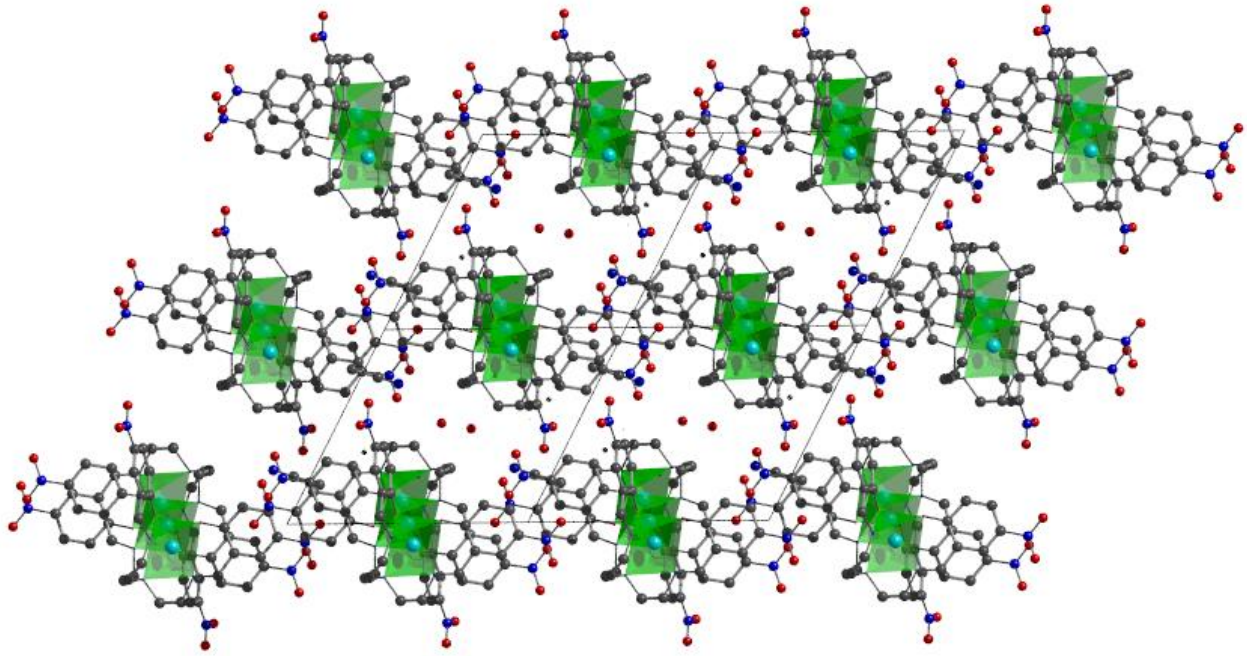

Figure S13. Packing diagram of compound **2**, along b–axis showing the chains like arrangement of molecules.

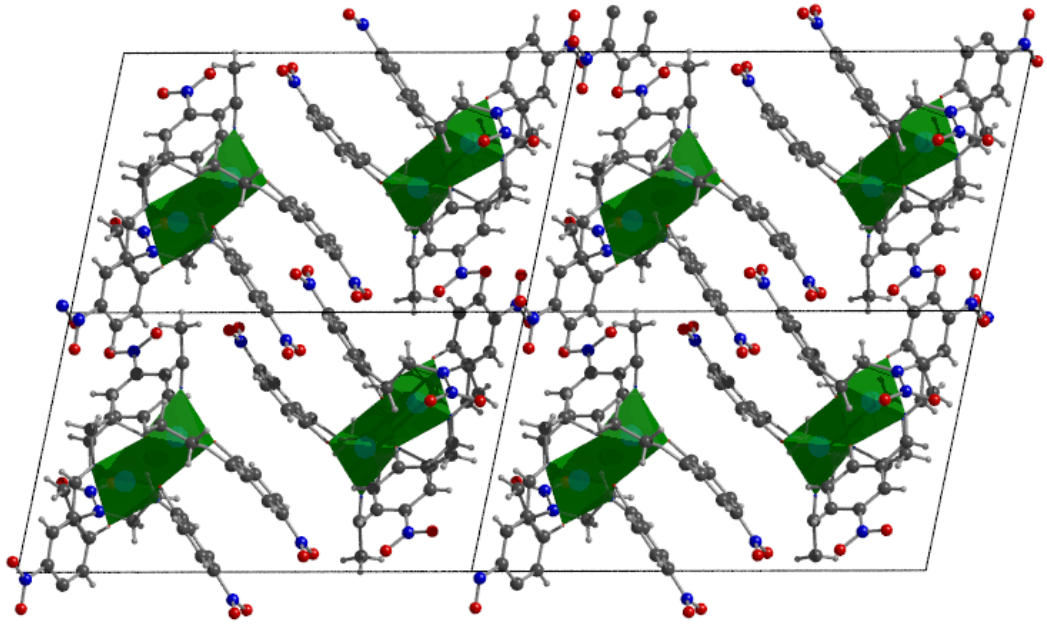

Figure S14. Packing diagram of compound **3** showing the chains of molecules running along along a–axis.

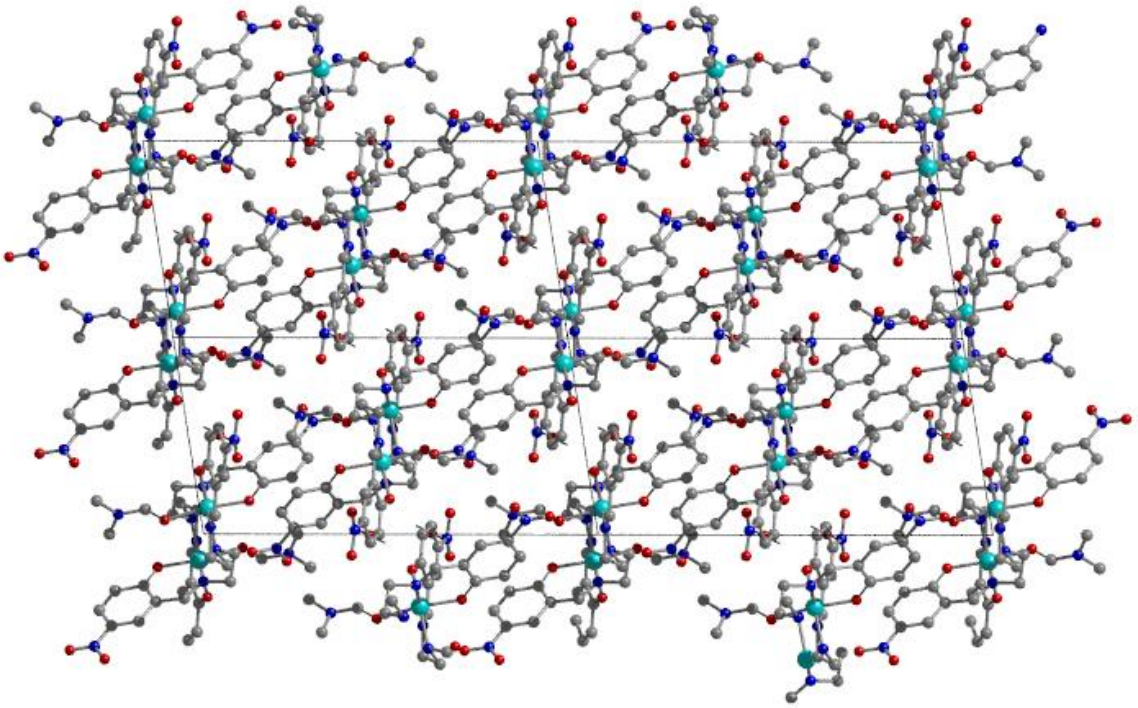

Figure 15. Packing diagram of compound **5** showing the chains of molecules running along along b–axis.

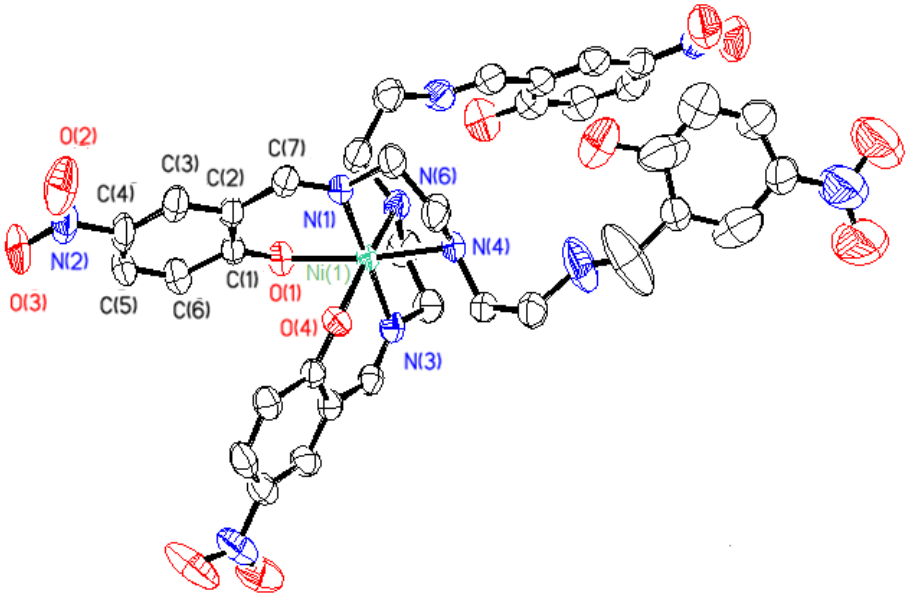

Figure S16. ORTEP diagram of $[Ni(HL^2)_2]\cdot H_2O$ **(6)**with 40% probability thermal ellipsoids and the atom-numbering scheme (hydrogen atom and water molecules are removed for clarity).

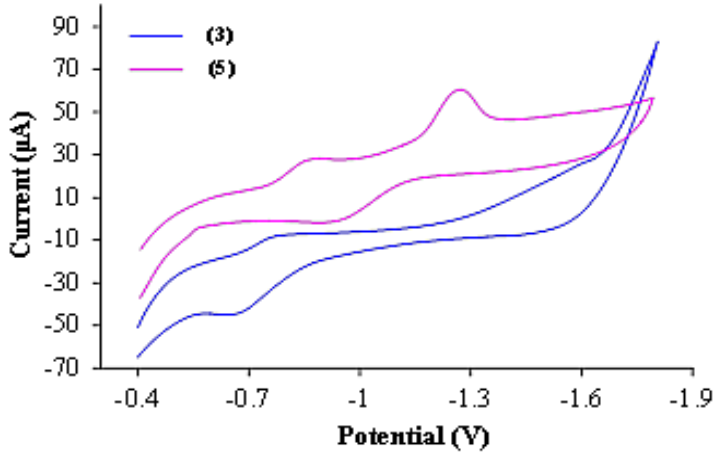

Figure S17(a). Cyclic voltammogram of complex **3** and **5 (**negative potential region) in 30% DMF-H_2O solution.

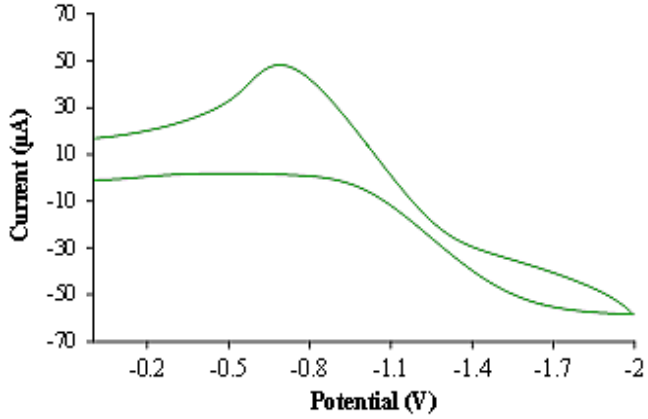

Figure S17(b). Cyclic voltammogram of complex **6 (**negative potential region) in 30% DMF-H_2O solution

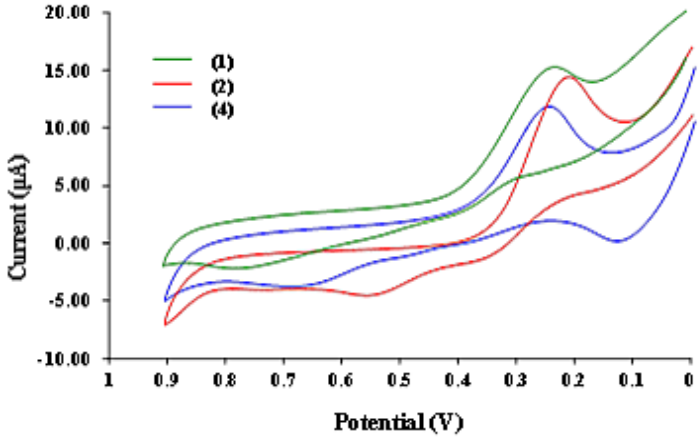

Figure S18 (a). Cyclic voltammogram of complex **1, 2** and **4 (**positive potential region) in 30% DMF-H_2O solution

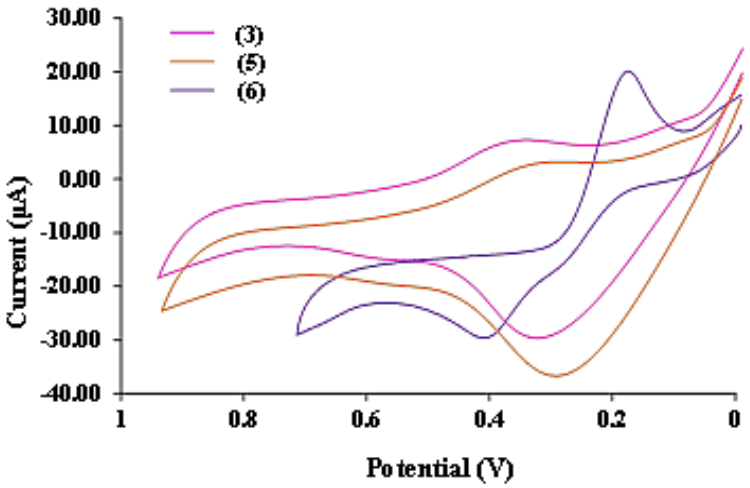

Figure S18 (b). Cyclic voltammogram of complex **3, 5** and **6 (**positive potential region) in 30% DMF-H_2O solution

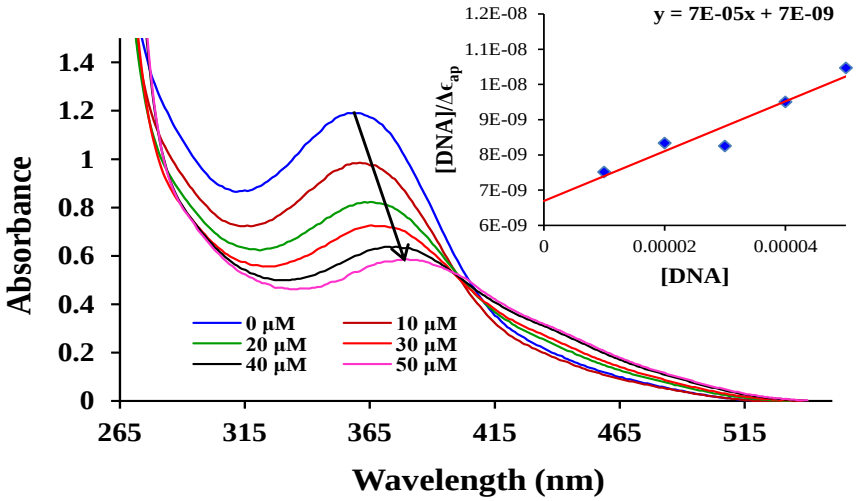

Figure S19. Absorption spectral changes at 356 nm (ε = 11900 $M^{-1}cm^{-1}$) upon the incremental addition of CT-DNA (0-50 μM) to complex **1** (100 μM, 1.0 mL) in 50 mM Tris-HCl/NaCl buffered 10% DMF solution (7.5 pH) at room temperature. Inset: Plot of [DNA]/$\Delta\varepsilon$ versus [DNA] obtained by the absorption titration of CT-DNA with Ni(II) complex.

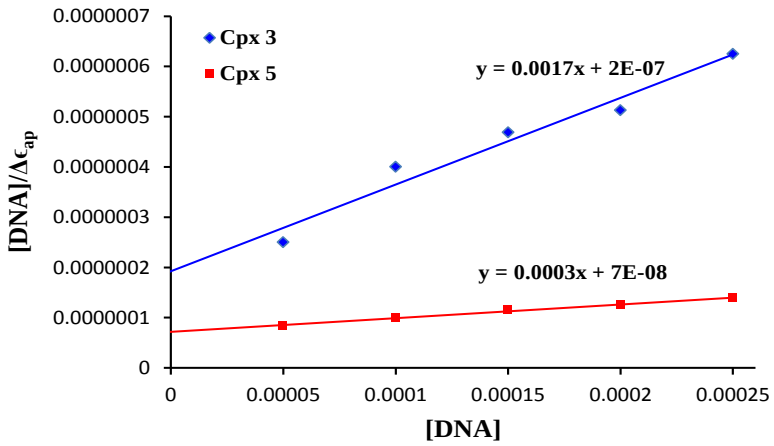

Figure 20(a). Plot of [DNA]/Δε versus [DNA] obtained by the absorption titration of CT-DNA with **3** and **5**.

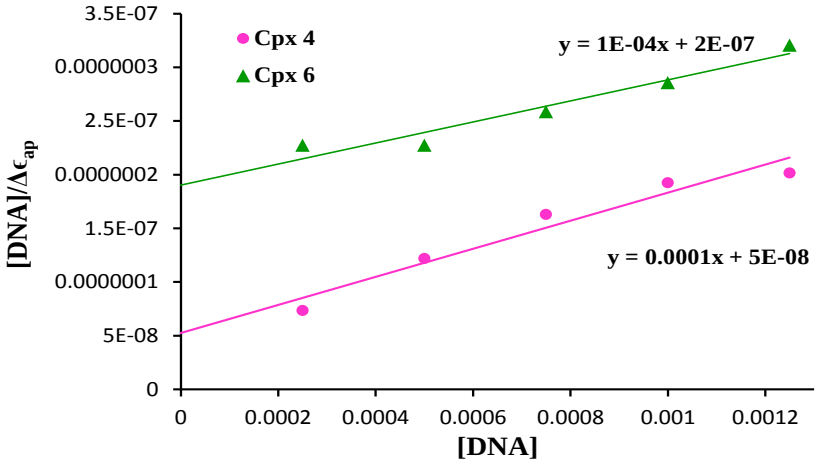

Figure 20(a). Plot of [DNA]/Δε versus [DNA] obtained by the absorption titration of CT-DNA with **4** and **6**.

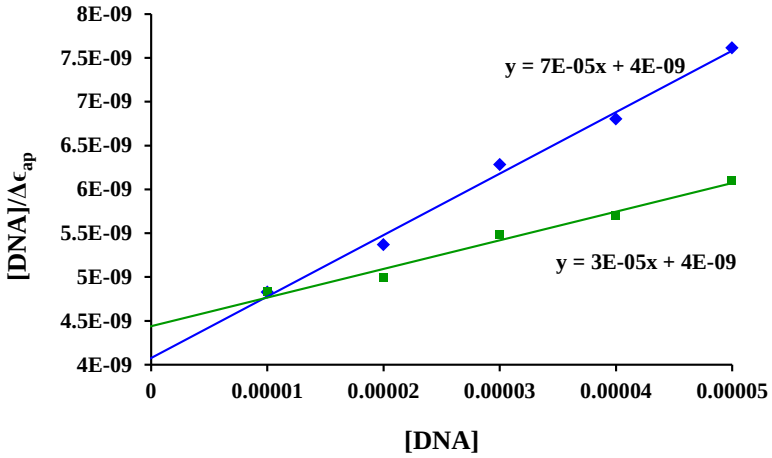

Figure S21. Plot of [DNA]/Δε versus [DNA] obtained by the absorption titration of CT-DNA with **2** in the absence (Blue) and presence (Green) of 100 mM NaCl solution in 20 mM phosphate buffer at 7.5 pH.

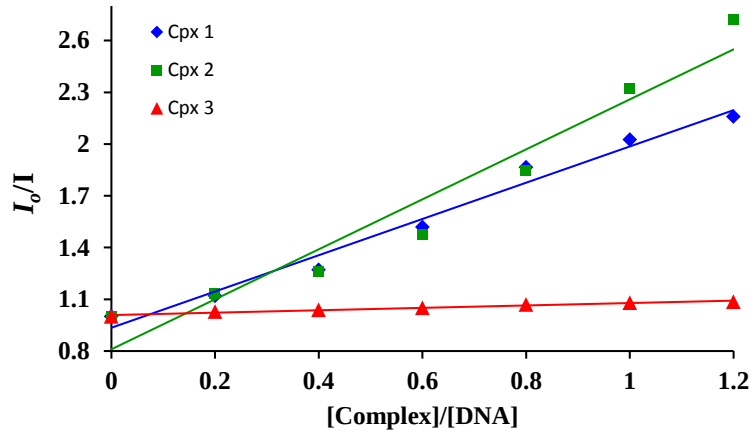

Figure S22. A comparison of emission intensity I_o/I *vs.* [Complex]/[DNA] for **1**, **2** and **3**.

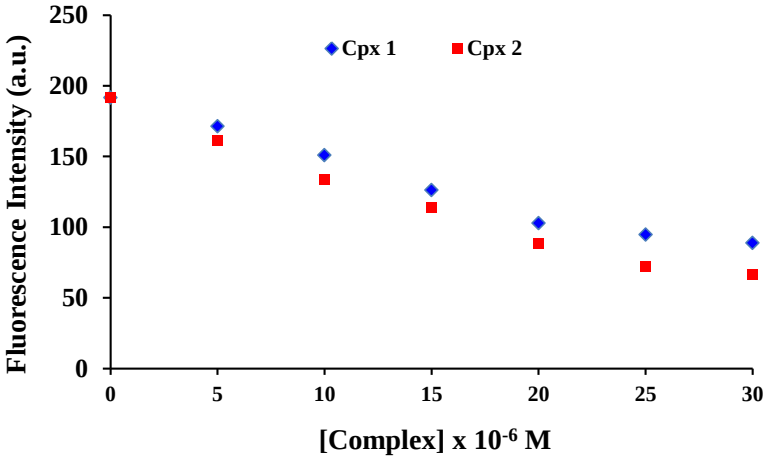

Figure S23. The effect of addition of complexes **1** and **2** (0-30 μM) on the emission intensity of EB (1.25 μM) bound to CT-DNA (25 μM) at 604 nm (λ_{ex}= 525 nm), in 50 Mm Tris-HCl/NaCl buffered 10% DMF solution (7.5 pH) at room temperature.

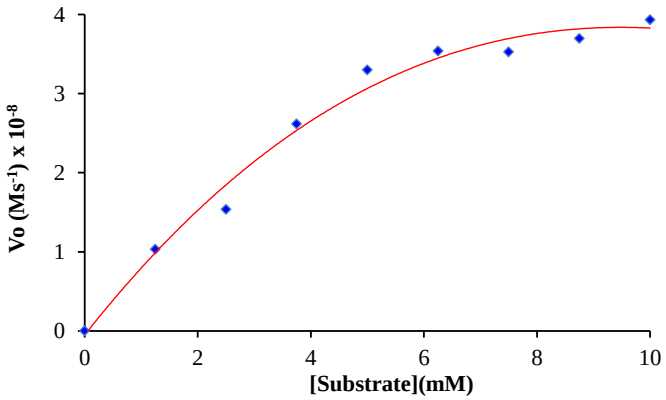

Figure S24 (a). Dependence of rate of transesterification on substrate concentration (0 -10 mM) for complex **1** (5×10^{-5} M) at 25 ^{o}C in 30% DMF (pH 8.5).

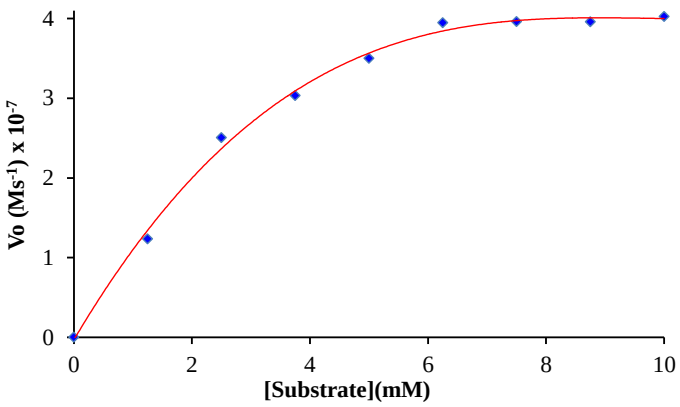

Figure S24 (b). Dependence of rate of transesterification on substrate concentration (0-10 mM) for complex **4** (5×10^{-5} M) at 25°C in 30% DMF (pH 8.5).

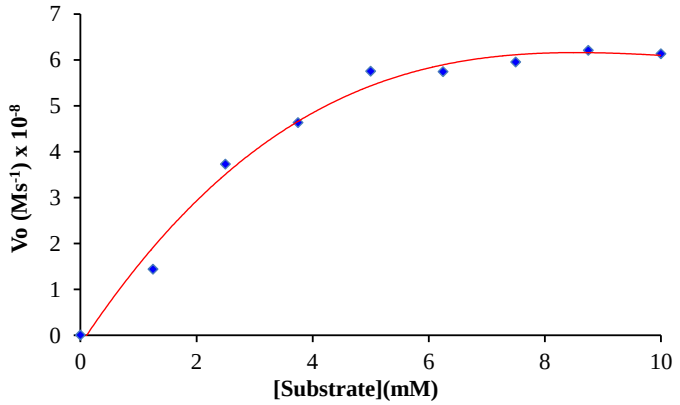

Figure S24 (c). Dependence of rate of transesterification on substrate concentration (0 -10 mM) for complex **5** (5×10^{-5} M) at 25°C in 30% DMF (pH 8.5).

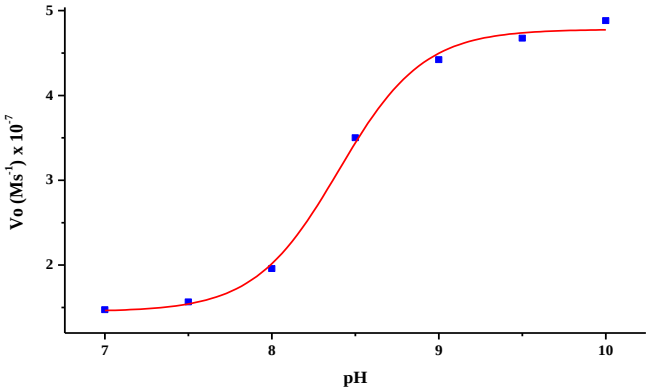

Figure S25. Dependence of the rate of 4-NPP hydrolysis on pH by complex **$[Ni_2(L^2)_2(H_2O)_2]$ (4).** [Complex]= 5×10^{-5}M; [BNPP]=5×10^{-3} M in DMF-H_2O (30%, v/v) at 25 °C.

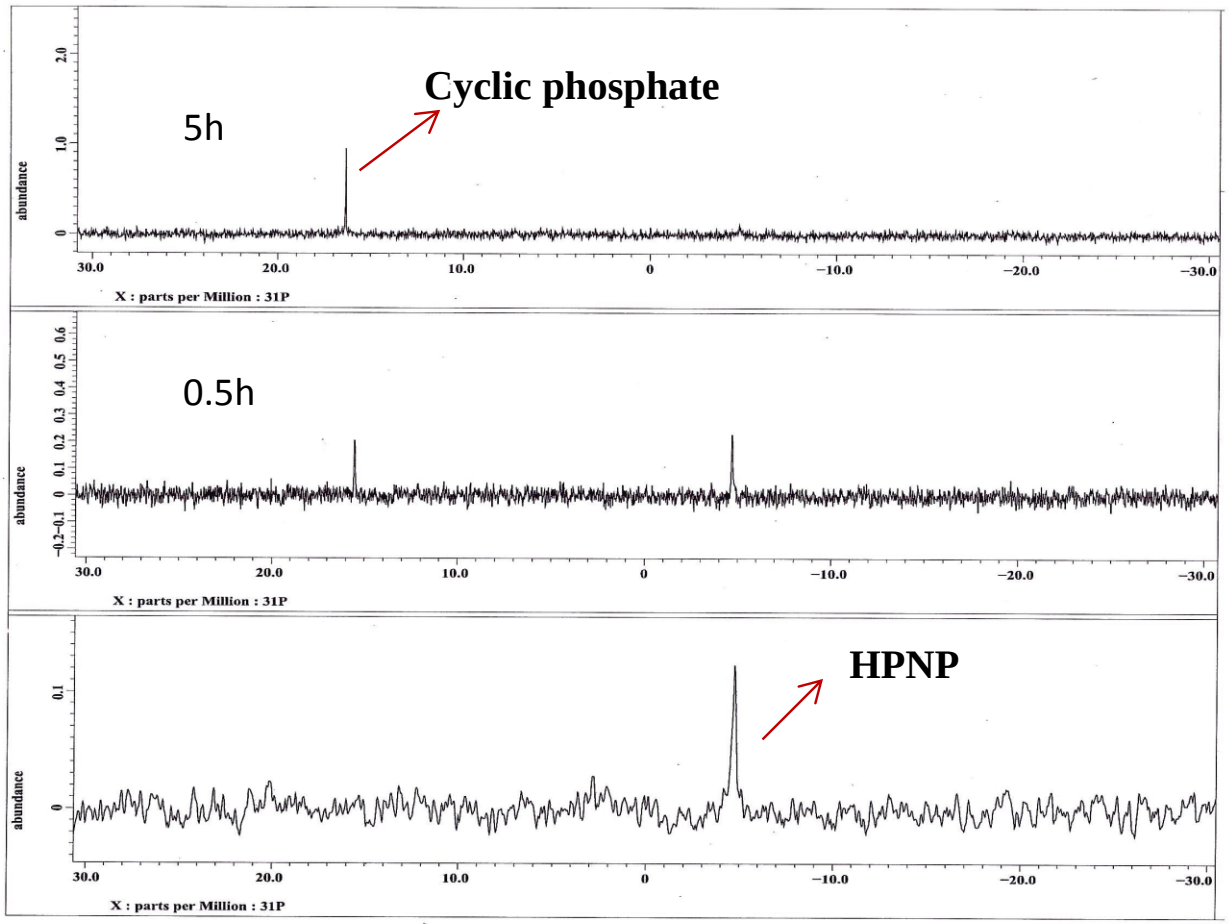

Figure S26. ^{31}P NMR of HPNP on addition of 0.1 mM solution of complex **3** in DMSO-d_6 (pH 8.5 in the presence of 0.1 M CHES buffer).

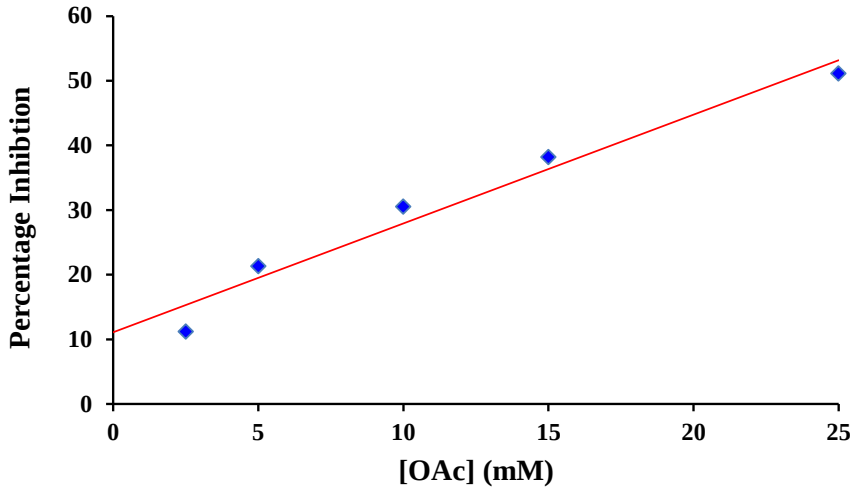

Figure S27. Percentage inhibition of HPNP hydrolysis with increasing concentration of acetate ion (2.5-25 mM) for complex **1** (percentage inhibition = [(normal activity - inhibited activity) / (normal activity)] ×100).

Table S1. Hydrogen bonding parameters (Å, ^{o}) of (**2)**

D-H···A	**D···A/ Å**	**H···A/ Å**	**D-H···A/^{o}**
C7-H7A...N8 ^{i}	3.463(7)	2.548(6)	167.9(3)
C9-H9A...O3 ^{ii}	3.362(4)	2.484(3)	150.5(2)
C10-H10B...O9 ^{iii}	3.277(6)	2.503(4)	136.7(2)
C15-H15A...O1	3.269(4)	2.523(2)	137.4(2)
C27-H27A...O5 I^{v}	3.191(5)	2.522(3)	129.1(3)
C28-H28A...O8 ^{v}	3.186(7)	2.503(4)	128.1(3)

Equivalent positions: (i) x,+y-1,+z, (ii)-x,-y,-z+2, (iii) x,+y,+z+1, (Iv)x+1,+y,+z-1, (v)-x,-y+1,-z+1

Table S2. Hydrogen bonding parameters (Å, ^{o}) of (**3)**

D-H···A	**D···A/ Å**	**H···A/ Å**	**D-H···A/^{o}**
N1-H1A...O13 ^{i}	3.100(8)	2.413(5)	132.4(3)
C1-H1A...O2 ^{i}	3.276(8)	2.546(5)	132.1(4)
C2 -H21A...O10 ^{ii}	3.444(8)	2.535(5)	166.0(4)
C5-H5A...O14 ^{iii}	3.351(8)	2.648(5)	132.8(4)
C14-H14A...O11 ^{iv}	3.468(10)	2.642(6)	148.2(5)
C19-H19B...O8 ^{v}	3.232(9)	2.512(6)	130.9(4)
C25-H25A...O4 ^{iv}	3.511(10)	2.665(7)	151.5(5)
C28-H28A...O3	3.132(8)	2.454(4)	127.8(4)
C29-H29B...O2 ^{vi}	3.200(8)	2.412(5)	138.1(4)
C30-H30A...O14 ^{vii}	3.410(8)	2.531(5)	157.7(4)
C34-H34A...O5 ^{viii}	3.406(9)	2.488(6)	169.3(4)
C35-H35A...O6	3.236(8)	2.550(5)	130.8(4)
C38-H38A...O8 ^{iii}	3.284(11)	2.641(6)	124.7(6)
C38-H38C...O4 ^{ix}	3.097(13)	2.157(7)	166.9(6)

Equivalent positions: (i) x,+y+1,+z (ii) -x,-y,-z+1, (iii) x+1,+y,+z, (iv) -x+1,-y,-z+1, (v) x,+y-1,+z, (vi) -x+1,-y,-z+2, (vii) -x,-y+1,-z+2, (viii) -x,-y+1,-z+1, (ix) -x+1,-y+1,-z+1.

Table S3. Hydrogen bonding parameters (Å, °) of (**5)**

D-H···A	**D···A/ Å**	**H···A/ Å**	**D-H···A/°**
O1W-H1A...O1	2.780(4)	1.926(2)	162.95(2)
O1W-H2A...O3 [i]	3.035(3)	2.208(2)	152.4(1)
C3-H3B...O5 [ii]	3.636(4)	2.714(3)	171.3(2)
C7-H7A...O5 [iii]	3.247(4)	2.431(3)	146.4(2)
C8-H8A...O3 [iv]	3.295(4)	2.603(2)	128.5(2)
C12-H12A...O1W [v]	3.761(3)	2.928(2)	161.4(2)
C20-H20A...O2 [i]	3.570(5)	2.628(3)	167.0(2)
C20-H20C...O4 [vi]	3.407(6)	2.524(4)	152.9(3)

Equivalent positions: (i) -x+2,-y+1,-z+1 (ii) x+1/2+1,-y+1/2,+z+1/2, (iii) x+1/2,-y+1/2,+z+1/2, (iv) -x+1,-y+1,-z+1, (v) x-1,+y,+z, (vi) x+1,+y,+z

Table S4. Crystal data and refinement parameters of $[Ni(HL^2)_2]\cdot H_2O$ **(6)**

Compound	**6**
Empirical Formula	$C_{36}H_{38}N_{10}NiO_{13}$
M_w	877.44
Temperature [K]	293(2)
Crystal System	Triclinic
Space group	*P*-1
a/ [Å]	11.6522(7)
b/ [Å]	19.4039(14)
c /[Å]	20.5549(15)
α/ [°]	69.909(3)
β /[°]	73.913(3)
γ/ [°]	83.331(3)
V [$Å^3$]	4192.6(5)
Z	4
D_c [Mg m^{-3}]	1.5303
μ / [mm^{-1}]	0.553
Reflections collected	166113
Data / restraints / parameters	20895/0/1190
Unique reflections, [R_{int}]	20895 [0.0755]
GOF = S_{all}	1.087
Final *R* indices	
R_1, wR_2 [I>2σI]	0.0768, 0.2211
R_1, wR_2 (all data)	0.1353, 0.2781
Δρmax/Δρmin[$Å^3$]	1.61/-1.14

Table S5. Selected bond lengths and angles (Å,º) for **(6)**

Bond lengths (Å)			
Ni-O(1)	2.054(3)	Ni-O(4)	2.047(3)
Ni-N(1)	2.009(3)	Ni- N(3)	2.014(3)
Ni- N(4)	2.204(3))	Ni- N(6)	2.138(3)
Bond angles (º)			
N(1)-Ni-N(3)	177.85(13)	N(1)- Ni-N(4)	81.43(12)
N(6)- Ni-N(3)	82.99(13)	N(6)-Ni-N(4)	9 93.91(13)
N(6)-Ni-N(1)	99.15(14)	O(1)-Ni-N(3)	91.99(12)
O(1)-Ni-N(4)	169.37(12)	O(1)-Ni-N(1)	88.18(12)
O(1)-Ni-N(6)	89.94(12)	O(4)-Ni-N(3)	8.47(12)
O(4)Ni-N(4)	90.13(12)	O(4) Ni-N(1)	89.39(12)
O(4)-Ni1-N(6)	171.00(13)	O(4)-Ni1-O(1)	87.49(11)